Bohl T, Tian G, Smallbone A, Roskilly AP.

Macroscopic spray characteristics of next-generation bio-derived diesel fuels in comparison to mineral diesel.

***Applied Energy* (2016)**

DOI: http://dx.doi.org/10.1016/j.apenergy.2016.10.082

Applied Energy xxx (2016) xxx–xxx

Contents lists available at ScienceDirect

Applied Energy

journal homepage: www.elsevier.com/locate/apenergy

Macroscopic spray characteristics of next-generation bio-derived diesel fuels in comparison to mineral diesel

Thomas Bohl, Guohong Tian, Andrew Smallbone *, Anthony P. Roskilly

Sir Joseph Swan Centre for Energy Research, Newcastle University, Newcastle upon Tyne NE1 7RU, UK

HIGHLIGHTS

- We present the macroscopic spray characteristics at engine-like (70 bar) conditions.
- Results are presented for four biodiesels and compared with mineral diesel.
- HVO had the lowest density and achieves the shortest penetration distance by 5%.
- Fuel liquid viscosity was a significant factor on the observed air-fuel mixing process.
- The Hiroyasu & Arai spray model was extended to include alternative bio-fuels.

ARTICLE INFO

Article history:
Received 23 May 2016
Received in revised form 22 September 2016
Accepted 24 October 2016
Available online xxxx

Keywords:
Biodiesel
HVO
Spray penetration
Spray cone angle
Spray area
Constant volume vessel

ABSTRACT

In this paper, the macroscopic spray characteristics of four next-generation biofuels, namely, hydro-treated vegetable oil (HVO), Palm oil methyl ester (PME), Soybean oil methyl ester (SME) and used cooking oil methyl ester (UCOME) were investigated in detail using a constant volume spray vessel, and benchmarked against reference mineral diesel (B0). During experiments, fuels were heated to 80 °C to achieve an engine-like environment before being injected at various compression ignition engine relevant operating conditions. The fuel spray tip penetration, spray cone angle and spray area were investigated analysing images obtained using a direct photography technique. Furthermore, a modified spray model was proposed to extend its scope to include alternative fuels by considering fuel density as part of the spray model. The results show that HVO with the lowest density of all fuels achieves the shortest penetration distance and the highest cone angle, resulting in a more distributed fuel-air mixture. All fuels have very similar spray areas for the same injection conditions, but the specific spray area per injected mass is highest for HVO followed by the three methyl esters. It was concluded that the fuel liquid viscosity was a significant factor on the observed air-fuel mixing process. The spray characteristics were compared with our engine test results and can be used to explain observed engine behaviour when fuelled with biofuels.

1. Introduction

Corresponding carbon dioxide emissions have increased by 36% since 1990 [1] and world energy consumption is expected to increase by 30% by 2030 [2]. Transportation counts for 30% of the total worldwide consumption, is also expected to grow drastically. The transportation sector's major energy source is fossil fuel oil and it accounted for 22% of the total CO_2 emissions in 2008 [3]. The increasing carbon dioxide emissions as well as depleting reserves of fossil fuels are forcing policymakers to reduce our dependence on mineral fuels and implement progressive policies which promote the use of alternative fuels. In May 2003, the European Parliament introduced the biofuel Directive 2003/30/EC, which instructs member states to supply 2% of the transport fuel from renewable sources in 2005, 5.75% by 2010 and 10% by 2020, respectively [4].

Growing fossil fuel consumption combined with depleting reserves and increasing instability within oil-producing countries has historically led to significant rises in energy prices [5,6]. The energy demand will increase in all sectors, but most significantly in the use of automobiles [7,8]. Biofuels are considered to have the potential to alleviate problems of fossil fuel depletion, fuel dependency and greenhouse gas emissions at some extent.

Biofuel is derived through various production techniques and is produced from a variety of plants of different scales, it was

* Corresponding author.
E-mail address: andrew.smallbone@newcastle.ac.uk (A. Smallbone).

http://dx.doi.org/10.1016/j.apenergy.2016.10.082
0306-2619/

Nomenclature

A_1	spray model parameter	X	parameter to compensate the higher injection pressure and chamber density
B_1	spray model parameter	x	linear quadratic equation term
m	spray model parameter (density exponent)	y	linear quadratic equation term
d_0	spray nozzle diameter (m)	z	spray model parameter weighting factor of the fuel density effecting the penetration
ΔP	pressure difference across the nozzle (Pa)	ρ_g	the ambient gas density (kg/m^3)
S	spray penetration length (m)	ρ_l	liquid fuel density (kg/m^3)
t	time (s)		
t_b	spray breakup time (t)		

important to install a standard fuel quality to guarantee a stable engine performance [9]. As such biodiesel must comply with the international biodiesel standard specifications, which include either the American Standards for Testing Materials (ASTM D6751) or the European Union Standards for biodiesel fuel (EN 14214) [10].

The differing fuel properties of biodiesel, such as viscosity, cetane number, surface tension, density and calorific value will influence the spray and combustion characteristics and therefore the change the corresponding exhaust gas composition. Studies have shown that those fuels with higher viscosities can lead to reduced spray atomisation quality. Consequently, the average droplet diameter of the spray and the breakup time is increased [11–13]. This leads to incomplete combustion and carbon deposits on the cylinder walls. A common method to investigate the effect of various fuel properties on the injection, atomisation and combustion process is the optical investigation of the pure spray injection process uncoupled from the atomisation and combustion elements. The fuel injection is an important part of the engine combustion process as it influences the spray characteristics significantly, such as breakup length, spray tip penetration, cone angle and Sauter Mean Diameter (SMD). These data in turn can be used to provide details about the air-fuel mixing characteristics and potential wall impingement [14].

Gao et al. tested three types of biodiesel, (Jatropha, palm and used frying oil methyl ester) using an oil pump injection system and reported that with increasing biodiesel blends the penetration distance increased and the cone angle decreased due to higher viscosity causing poorer atomisation [15]. Kuti et al. investigated the spray characteristics of palm oil methyl ester (PME) and mineral diesel by injecting the fuel into constant volume vessel. They found that biodiesel injects further into the chamber than mineral diesel, which they explained with the higher boiling range of biodiesel [16]. Suh and Lee observed that biodiesel and its blends have a slower injection velocity compared to mineral diesel caused by the higher surface tension and viscosity. The lower velocity also led to increased mean droplet size diameters [17]. Grimaldi and Postrioti also investigated the spray characteristics of biodiesel and mineral diesel using a common-rail injection system and concluded likewise that higher viscosity and surface tension cause longer penetration as the atomisation process is poorer [18].

Although the above researchers have examined the spray characteristics of some biodiesels, this research topic remains incomplete as; (a) there are numerous bio-derived diesel fuels with newer variants under continual development (such as some of those presented here), (b) as fuel injection systems have advanced in their design towards delivering newer generations of compression ignition engines, corresponding fuel injection pressures have increased significantly thus fundamentally changing fuel spray characteristics and challenging the technical relevance of much of the historical evidence collected previously; and (c) the effect of these fuel properties in combination with optimising the fuel injection events themselves has not been considered in detail. In this work, the above challenges have been addressed through obtaining new experimental data for a new generation of biodiesels at real-world and state-of-the-art engine injection pressures (1800 bar). Results of the fuel injector calibration have been obtained at the same injection conditions for cross-comparison and have been applied to the spray test results to address the differences in fuel properties and analyse how these impact on the quality of the spray itself.

As a means to further explore the importance of these characteristics, a theoretical spray model has been applied and modified to extend its applicability to the higher injection and back pressures used in state-of-the-art internal combustion engines. The fuel density affecting the penetration distance has been used to extend the model to provide a better overall robustness when being used for alternative fuels other than mineral diesel.

The results of this paper will be used by engine developers to better understand the spray characteristics of these biodiesel fuels in context with conventional mineral diesel fuel. It will support their research and development of fuel-flexible engines by offering new insight on these fuels at relevant conditions and therefore enable them to (i) better understand the differences in the fuels, (ii) design and simulate a more optimal injection strategy/engine and, (iii) facilitate the roll-out of more sustainable fuels and engine technologies.

2. Experimental setup and procedure

A medium pressure, high temperature combustion vessel filled with compressed nitrogen was used to investigate the spray characteristics using high-speed direct photography technique. The vessel is made of Inconel alloy and is resistant against corrosion and oxidation and suited for extreme environments subjected to pressure of 100 bar and temperatures of up to 1000 K. The constant volume vessel (CVV) has four optical accessible windows with 100 mm viewing size and further consists of an external 4.5 kW ceramic band heater to achieve background temperatures of up to 700 °C.

The fuel injection system contains an air-driven high pressure fuel pump, where the fuel can be pressurised and stored in a common rail up to 1800 bar. A standard Bosch solenoid injector with a 0.16 mm single-hole nozzle was mounted onto the vessel and was triggered by an external solenoid driving box. A PHANTOM V710 monochrome charge-coupled device (CCD) camera captured the spray images with a resolution of 256 × 256 pixels, using a capturing speed of 70,000 frames per second (fps) and an exposure time of 5 ns. The camera was synchronised with the injector by using the same triggering signal. A Nikon AF-S Nikkor lens with a focal length of 70–200 mm and a maximum aperture of f/2.8 was attached to the camera. A 500 W Xenon light source on the opposite window ensures constant background light for the camera. The background pressure and temperature of the vessel is monitored

Please cite this article in press as: Bohl T et al. Macroscopic spray characteristics of next-generation bio-derived diesel fuels in comparison to mineral diesel. Appl Energy (2016), http://dx.doi.org/10.1016/j.apenergy.2016.10.082

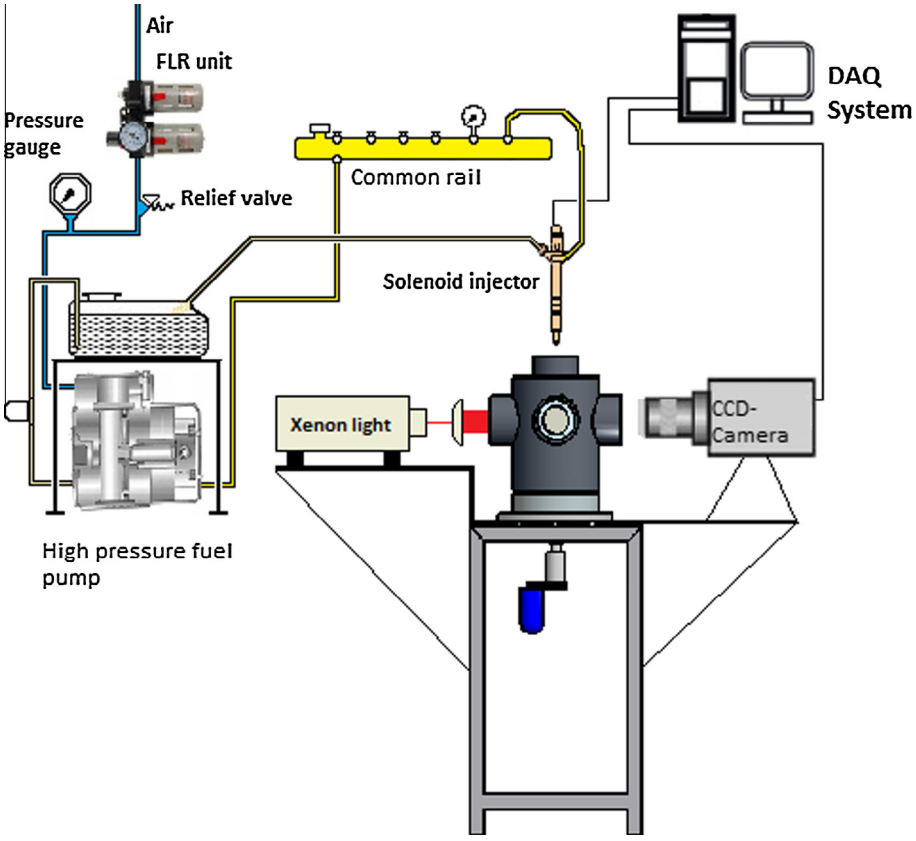

Fig. 1. Constant volume vessel set up.

Fig. 2. Sequence of detected images at 1800 bar injection pressure and 65.5 kg/m^3 chamber density.

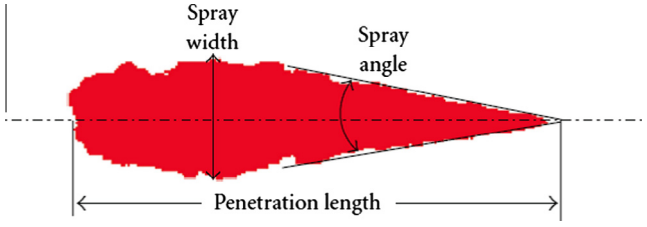

Fig. 3. Measurement points of macroscopic spray [19].

and controlled by a control panel. The CVV set up including high pressure fuel system and optical diagnostic devices are illustrated in Fig. 1.

A MATLAB program was developed to automatically measure cone angle, penetration length and spray area of batches of spray images such as those presented in Fig. 2. In Fig. 3 the two main spray characteristics are illustrated, these are cone angle and penetration length, measured by the program. The "Spray Tip Penetration Length" is defined as the distance between the nozzle exit and the furthest point of the spray.

The "Cone Angle" can be defined as the angle formed by two tangential lines touching the outer boundaries of the spray at either side and joining together at the nozzle exit. The cone angle was determined by measuring the angle between nozzle exit and

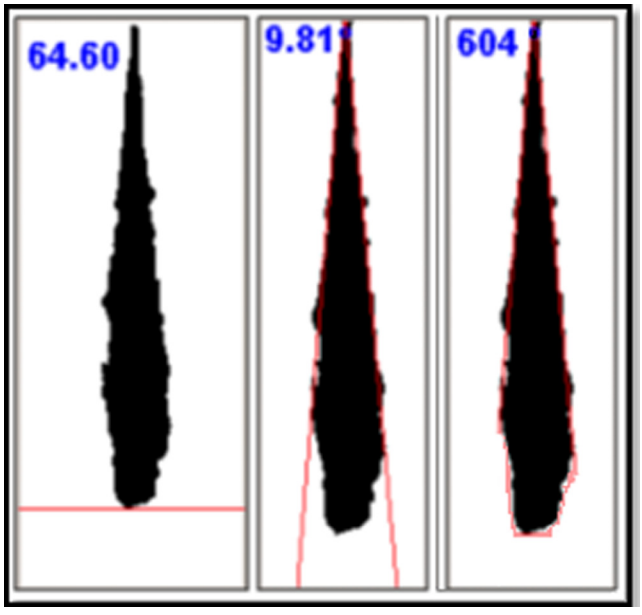

Fig. 4. Annotated spray measurements.

Please cite this article in press as: Bohl T et al. Macroscopic spray characteristics of next-generation bio-derived diesel fuels in comparison to mineral diesel. Appl Energy (2016), http://dx.doi.org/10.1016/j.apenergy.2016.10.082

Table 1
Main fuel properties of tested fuels.

Fuel	Density at 80 °C (kg/m^3)	Viscosity at 40 °C (mm^2/s)	Cetane number (–)	Calorific value (kJ/kg)
B0 mineral diesel	796.8	2.82	51	42,853
HVO B100	736.5	3.02	>75	43,902
PME B100	829.7	4.55	64.9	37,320
SME B100	838.4	4.18	53.7	37,230
UCOME B100	832.7	4.35	58.4	37,200

Table 2
Injector calibration results in mg per stroke.

Fuel	600 bar	1800 bar
B0 mineral diesel	2.60	6.32
HVO B100	2.33	5.61
PME B100	2.33	7.00
SME B100	2.25	6.97
UCOME B100	2.55	6.92

Table 3
Standard deviation of tip penetration at high and low injection pressures.

Fuel	600 bar	1800 bar
B0 Reference diesel [mm]	±0.829	±0.853
HVO B100 (mm)	±0.693	±0.616
PME B100 (mm)	±0.747	±1.024
SME B100 (mm)	±0.673	±0.869
UCOME B100 (mm)	±0.714	±0.959

the first and last pixel of each row and taking the average. The spray area is defined as the area covered by the fuel plume at chamber conditions. To calculate the spray area, the binary image with the same threshold limit as for the penetration and cone angle was used to sum up all black pixel within the spray plume. The principle is illustrated in Fig. 4 for the three measurements, penetration distance, cone angle and surface area.

The five test fuels in this work were reference diesel (B0), hydrotreated vegetable oil (HVO), palm oil methyl ester (PME), soybean methyl ester (SME) and used cooking oil methyl ester (UCOME). All fuels were provided as B100 neat fuels and B50 blended fuels together with their full Certification of Analysis. B0 has been chosen for benchmarking and validation purposes as it complies with the EN590 standard.

HVO is a so called "third generation" fuel and produced by adding hydrogen to vegetable oil via a catalytic process [19]. Its main characteristics are the very low fuel density and very high cetane number compared to other fuels due to its high paraffin content. Both, SME and PME are FAMEs (fatty acid methyl esters) and have the disadvantage of being food-competitive, meaning that their production occupy fertile farmland. UCOME was chosen as it is considered to be highly sustainable source as its feedstock is a waste material and therefore it is independent of the food vs. fuel debate. For the macroscopic spray tests the fuels were heated to 80 °C to have similar fuel temperatures to real engine conditions. High temperature injection was achieved by wrapping a robe heater around the injector. The fuel return temperature straight after the injector return outlet was measured and assumed to be identical with the fuel injection temperature. The most important fuel properties are presented in Table 1.

3. Results and discussion

3.1. Injector calibration

To determine the injected fuel quantity per stroke, a single-hole nozzle with an orifice diameter of 0.16 mm was selected. Calibration was carried out at 80 °C fuel temperatures, 600 bar and

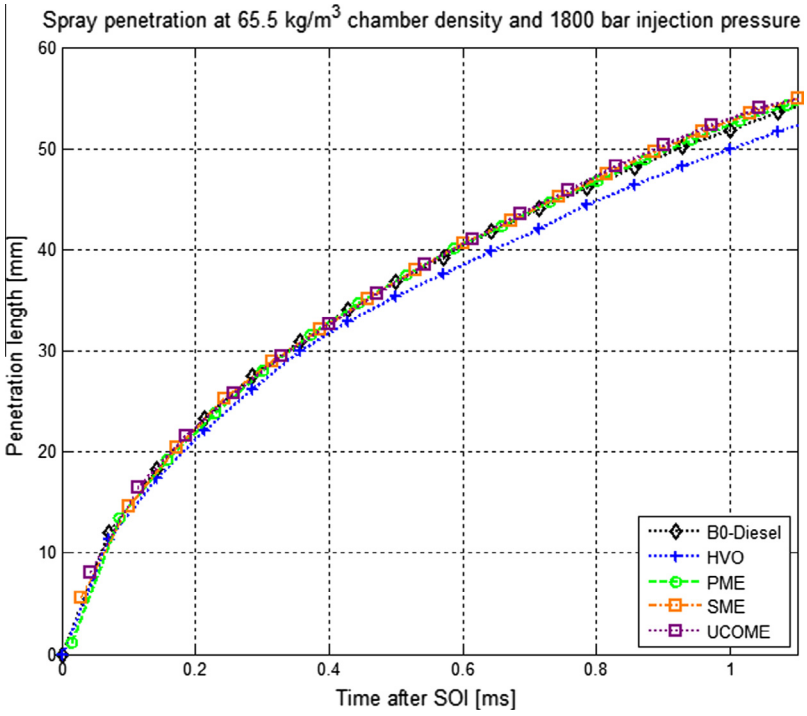

Fig. 5. Spray penetration at 100 °C and 70 bar backpressure.

Please cite this article in press as: Bohl T et al. Macroscopic spray characteristics of next-generation bio-derived diesel fuels in comparison to mineral diesel. Appl Energy (2016), http://dx.doi.org/10.1016/j.apenergy.2016.10.082

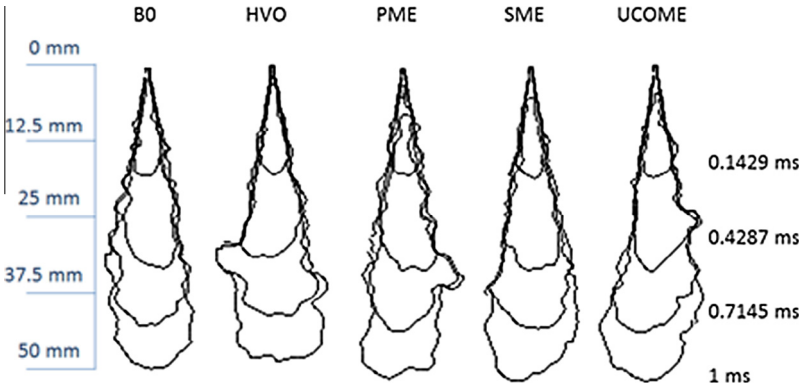

Fig. 6. Spray evolution of various (bio)-diesel at 100 °C chamber temperature.

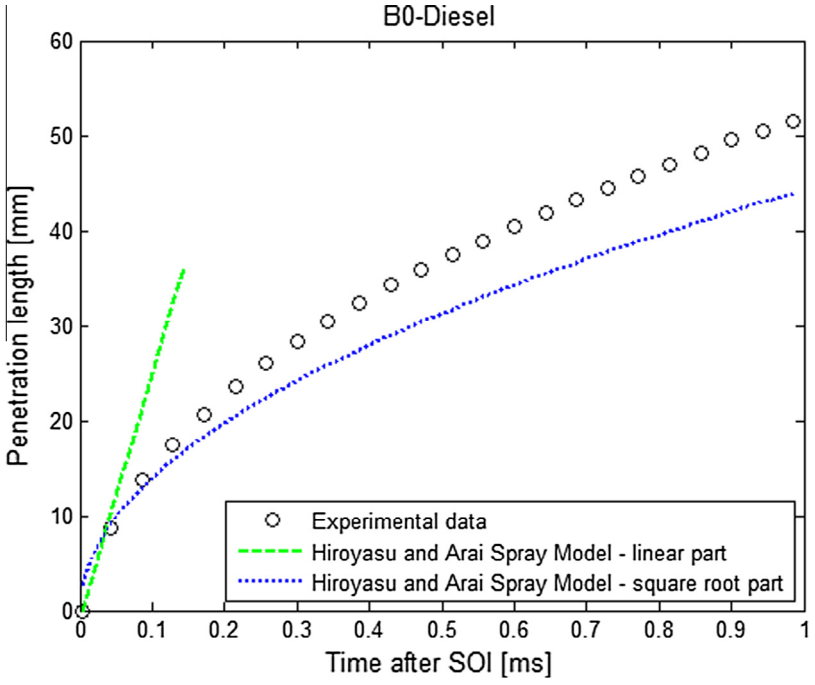

Fig. 7. Experimental spray data and Hiroyasu model for B0 diesel at 1800 bar injection pressure.

1800 bar injection pressure, and 0.6 ms injection duration. The main reason for choosing this injection duration was that this will approximately represent the injection duration on the Cummins 4 cylinder, 210 HP heavy duty test engine installed at the Sir Joseph Swan Centre at Newcastle University. The eight holes of the solenoid injectors have a 0.17 mm bore size and at average speed of 2000 rpm, the 0.6 ms injection duration is equivalent to 7.2 CAD resulting in somewhere between 30 and 50% engine load depending on rail pressure. To measure the injected mass per stroke the fuel was injected 1000 times in a measuring cylinder filled with fuel absorber and the weight of the cylinder was measured before and after the process. Each calibration has been repeated four times, averaged and divided by the total injection number to gain the mean mass per single injection.

The same fuel injection system was used for both calibration and spray tests.

At 100 °C chamber temperature, the fuel temperature is about 80 °C as the fuel in the injector heats up by heat transfer from the vessel. With higher fuel temperatures the viscosity drops and the density increases, which favours penetration velocity and cone angle. However a parametric investigation showed that the trends presented below proved largely to be independent of the vessel temperature, as such results are only presented with a chamber temperature of 100 °C.

The calibration results for 600 and 1800 bar injection pressure are shown in Table 2. At high injection pressures the amount of mass injected per stroke is proportional to the fuel density, resulting in a higher mass per stroke for biodiesel and low injection amount for HVO with a significantly lower density. At low injection pressure of 600 bar the fuel density seem to play a relatively weaker role on the injection quantity and the high viscosity of biodiesel is likely to cause unstable fuel injection quantities. With increasing rail pressure the injection quantity increases significantly.

3.2. Spray tests

For the spray tests the same injector was used. The chamber was heated to 100 °C and the back pressure was set to 70 bar resulting in a chamber density of 65.5 kg/m^3. The two injection pressures were 600 bar and 1800 bar with an injection duration of 0.6 ms.

Please cite this article in press as: Bohl T et al. Macroscopic spray characteristics of next-generation bio-derived diesel fuels in comparison to mineral diesel. Appl Energy (2016), http://dx.doi.org/10.1016/j.apenergy.2016.10.082

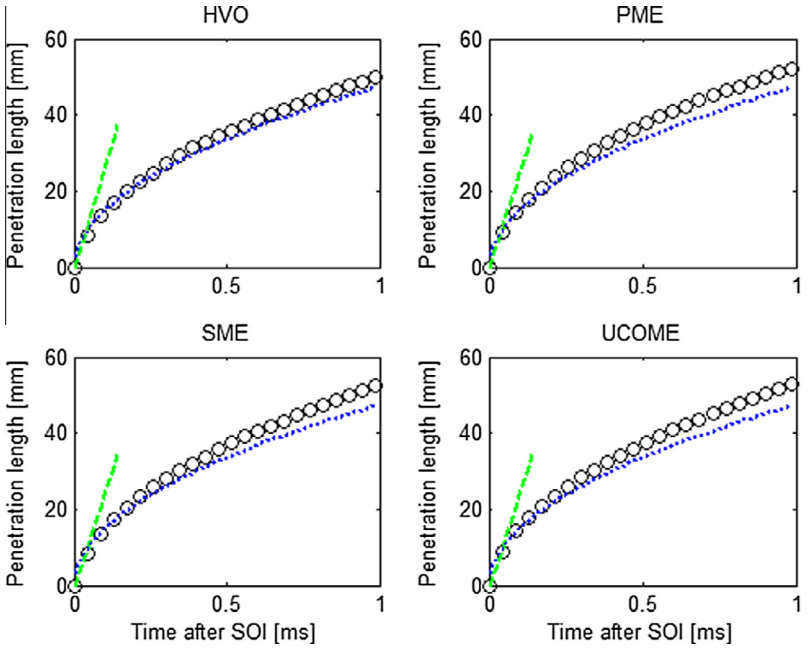

Fig. 8. Experimental spray data and Hiroyasu model for various (bio)-diesel at 1800 bar injection pressure.

Table 4
Correlation factors and coefficient of determination of fuel penetration trend lines.

Fuel	A_2	B_2	R^2
B0 Reference diesel	53.087	0.5386	0.9982
HVO B100	51.337	0.5474	0.9973
PME B100	53.524	0.5333	0.9988
SME B100	53.602	0.5524	0.9984
UCOME B100	53.807	0.5443	0.9984
HVO B50	52.298	0.5389	0.9948
PME B50	53.570	0.5426	0.9870
SME B50	53.203	0.5515	0.9828
UCOME B50	53.427	0.5398	0.9902

Table 5
Linearised x- and y-values for the graphical equation solution.

Fuel	$\ln(\rho)$	A_2/A_1	$\ln(A_2/A_1)$
B0 Reference Diesel	6.681	1.1157	0.1095
HVO B100	6.602	1.0790	0.0760
PME B100	6.721	1.1249	0.1177
SME B100	6.731	1.1266	0.1192
UCOME B100	6.725	1.1309	0.1230
HVO B50	6.642	1.0992	0.0945
PME B50	6.701	1.1259	0.1186
SME B50	6.706	1.1182	0.1117
UCOME B50	6.703	1.1229	0.1159

The data were averaged for ten sets of 70 images and the standard deviation was obtained. As the main focus of this work is placed on investigating the effect of various biodiesel the changes in spray characteristics have been analysed for the neat fuels (B100) and their blends (B50) with diesel. As the start of the visible fuel injection was different for data set every first image with a visible injection has been referenced to zero for all fuels.

3.2.1. Spray tip penetration

Fig. 5 shows the spray tip penetration of mineral diesel and the four neat biofuels (B100 series) for the high injection pressures of 1800 bar (only every fifth data point has been plotted to have a better distinction between the curves). It shows that the higher density fuels, SME, PME and UCOME have longer tip penetration and HVO with a relatively low density has a shorter penetration distance. This observation is in agreement with the work of other researchers investigating the macroscopic characteristics of other biodiesel fuels [20–22].

The standard deviation (STD) of the penetration has not been included in the chart, but the averaged STD of each fuel is illustrated in Table 3. The STD values in the table indicate that at lower injection pressures the deviation is significantly lower for the three FAMEs. HVO shows the lowest STD of all fuels at 1800 bar followed by mineral diesel and SME. PME deviates the most, potentially due to its relatively high viscosity. In general, the standard deviation is higher at high injection pressures, it was considered that this was because the total penetration length is longer resulting in a corresponding larger absolute deviation.

Fig. 6 presents the spray evolution process of all neat fuels at 1800 bar injection pressure. The penetration tip is longer for all three FAMEs, PME, SME and UCOME; however at the start of injection all fuels still have similar penetration trends and the differences grow as the injection event evolves. Also it can be seen that the cone angle becomes constant over time. At 1 ms after injection, the three FAMEs are already broken up from the nozzle while HVO and mineral diesel still show a complete spray plume at the tip of the nozzle. The reasons for earlier injection breakup cannot be explained at this stage, however the influence of the higher viscosity is evident on the break-up.

3.2.2. Spray tip penetration model

Researchers developed or adopted theoretical models of spray penetration to verify experimental results and evaluate their reliability with the phenomenological spray models [21,23–25]. Phenomenological models are integrations of reduced physics-based methods and experimental data, in spray applications this combination has resulted in many derivatives of such models with very few differences aside from the relevance of data used in their calibration. One very well established model is that of Hiroyasu and Arai, which was adopted to analyse the experimental penetra-

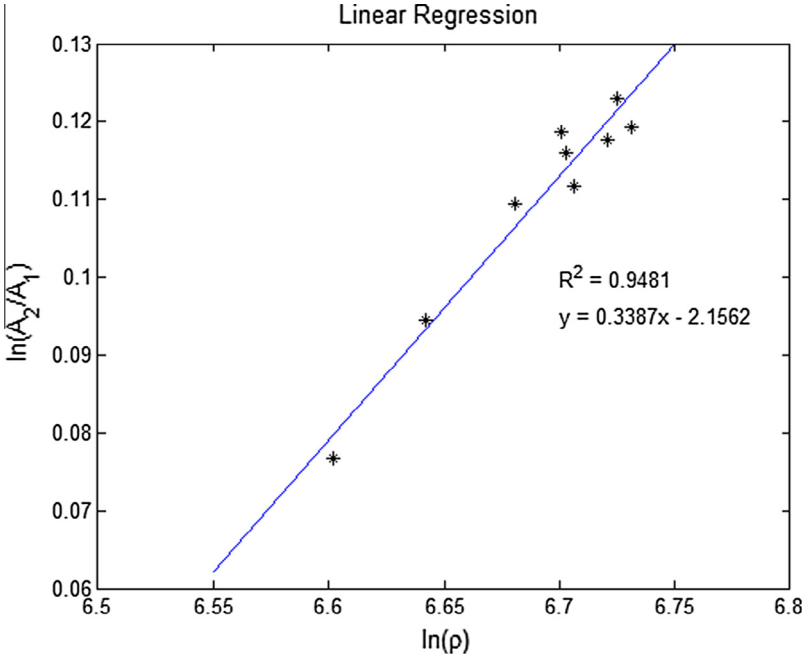

Fig. 9. Graphical solution of the density dependency on spray penetration.

tion curves and to evaluate the validity of this model for the use of different biofuels [23]. This model was selected for further analysis in this work above the many other candidates because historically it is so well established for fuel spray applications (*i.e.* accessibility within CFD codes, textbooks etc.), simplicity and its distinctive input parameters. Furthermore, it was considered that whilst other phenomenological spray models [21,23–25] might also be appropriate, the assumptions, numerical approaches *etc.* are similar enough that the general outcomes and conclusions of this work would be identical. The Naber and Siebers model, which is based on the principles of the Hiroyasu and Arai model, was also been considered in detailed, however the results of this model showed insignificant differences in the spray penetration. Additionally, a greater number of input parameters were necessary and parameters such as the correct nozzle discharge coefficient and contraction coefficient could not be obtained with full confidence.

In the 1970s, Dent and Hay et al. published detailed comparisons of different spray models and concluded that models predicting the relationship between penetration distances to the square root of time give the best accuracy [25,26]. Although Dent established a model applying the gas jet mixing theory, while Wakuri's model related the spray angle to appropriate physical parameters, both models still incorporate the basic parameters pressure difference, gas density, nozzle diameter and square root of time [25,27,28]. It was Hiroyasu and Arai who first applied the two-zone theory saying that the penetration length is proportion to the time, t until the spray breaks up and then advance at a rate proportional to the square root of time. Many recently established spray models have been derived from these initial assumptions that the spray is influenced by the diesel injection system parameters and by the environment where the spray is injected into. With this many models are more or less derived from this original relationship established by Hiroyasu and Arai and they all carry these basic principles in their codes.

Although the theoretical model was verified at low back pressure and injection pressure only, the general principle of the model was believed to be valid for higher pressures as well. They established a correlation between the spray penetration, S and the time, t by considering two effects influencing the penetration process. At the start of the injection, the fuel density and injection pressure dominates the spray penetration, S, while with ongoing injection the air entrainment process in the chamber becomes more dominate. Hiroyasu et al. stated that the time when the chamber conditions become more dominate than the injection conditions is the breakup time, t_b [23]. The spray penetration up to the breakup time was considered to be a linear function of time, while the penetration after the initial breakup progresses with the square root behaviour. The linear and root function equation are shown in equation (Eq. (1)) and (Eq. (2)) [23]:

$$S_1 = 0.39 \cdot \left(\frac{2 \cdot \Delta P}{\rho_l}\right)^{\frac{1}{2}} \cdot t \quad for\ t < t_b \tag{1}$$

$$S_2 = 2.95 \cdot \left(\frac{\Delta P}{\rho_g}\right)^{\frac{1}{4}} \cdot \sqrt{d_0 \cdot t} \quad for\ t \geqslant t_b \tag{2}$$

S is the penetration (m); t, time (s); ΔP, pressure difference across the nozzle (Pa); ρ_l, liquid fuel density (kg/m^3); ρ_g, the ambient gas density (kg/m^3), and d_0 the nozzle diameter (m). Using the above equations, the comparison of the theoretical model and the experimental data at 1800 bar is illustrated in Figs. 7 and 8 (only every third data point has been plotted to have a better distinction between the curves).

In the Hiroyasu model, S_1 before break-up time seems still valid, but S_2 changes at higher injection and higher back pressure. As the

Table 6
New correlation factor for modified Hiroyasu and Arai spray model.

Fuel	Real A2	Calculated A2	B2
B0 Reference diesel	53.087	52.941	0.5386
HVO B100	51.337	51.549	0.5474
PME B100	53.524	53.672	0.5333
SME B100	53.602	53.862	0.5524
UCOME B100	53.807	53.738	0.5443
HVO B50	52.298	52.254	0.5389
PME B50	53.570	53.309	0.5426
SME B50	53.203	53.405	0.5515
UCOME B50	53.427	53.342	0.5398
Average:			**0.5432**

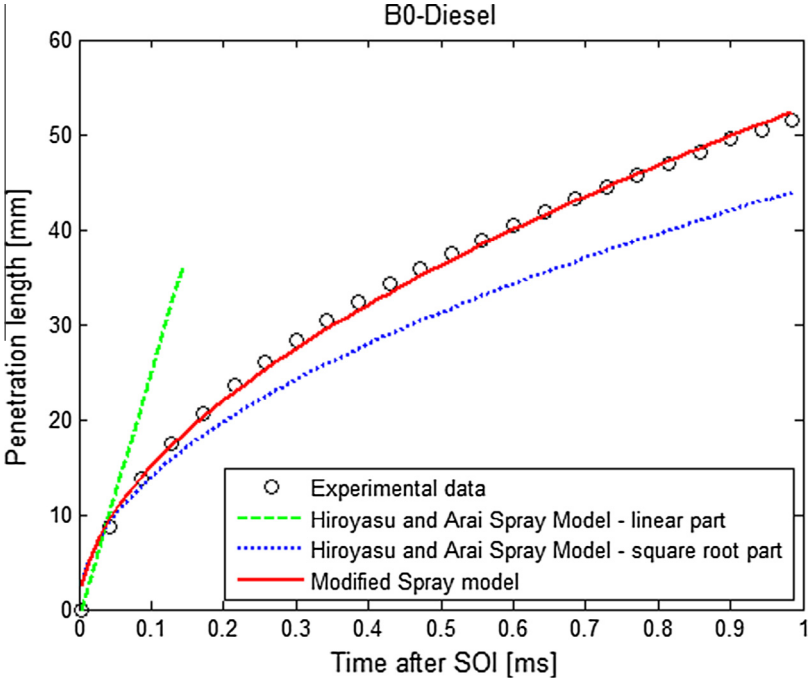

Fig. 10. Comparison between experimental spray data and modified Hiroyasu model for B0 diesel.

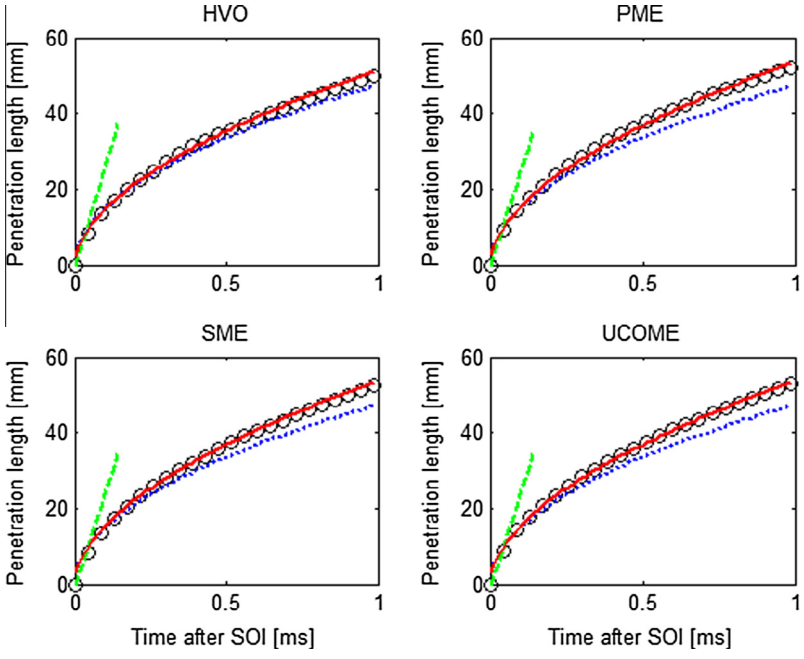

Fig. 11. Experimental spray data and modified Hiroyasu model for various (bio)-diesel at 1800 bar.

difference between the experimental data and the theoretical correlation is not constant for all fuels, it seems likely that at least one fuel parameter will have a significant effect on the spray penetration. For the linear correlation before break-up time, Hiroyasu and Arai have taken the fuel density into account, but for the root function after break-up time, the fuel density has not been considered. A hypothesis has been established saying that the fuel density will influence the penetration after the break-up time. To prove this new correlation, factors have to be determined and the weight of the fuel density within this equation has to be derived. According to Hiroyasu and Arai the two correlation factors for the root function are:

$$A_1 = 2.95 \cdot \left(\frac{\Delta P}{\rho_g}\right)^{\frac{1}{4}} \cdot \sqrt{d_0} \tag{3}$$

$$B_1 = 0.5$$

Thus the S_2 root function can be written as:

$$S_2 = A_1 \cdot t^{B_1} \tag{4}$$

Please cite this article in press as: Bohl T et al. Macroscopic spray characteristics of next-generation bio-derived diesel fuels in comparison to mineral diesel. Appl Energy (2016), http://dx.doi.org/10.1016/j.apenergy.2016.10.082

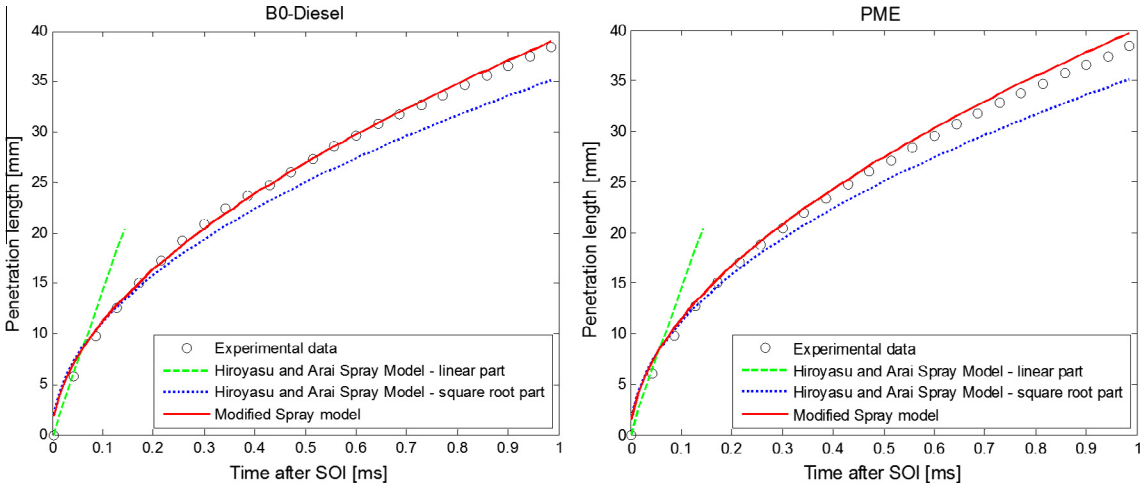

Fig. 12. Comparison of original and modified spray model at 600 bar injection pressure.

Table 7
Average spray cone angle at high and low injection pressures.

Fuel	600 bar	1800 bar
B0 Reference diesel	20.03	21.56
HVO B100	21.33	22.29
PME B100	19.81	21.1
SME B100	20.28	20.88
UCOME B100	19.89	21.62

The values for A_1 and B_1 are constant for all fuel types, as ΔP, ρ_g, and d_0 do not change when changing fuels. At 1800 bar injection pressure, 70 bar back pressure, 100 °C chamber temperature and 0.16 mm nozzle diameter the values for A_1 and B_1 are 47.58 and 0.5, respectively.

The experimental spray data has been plotted vs time (see Fig. 5) and a trend line in the format of the power equation (Eq. (4)) has been added with the experimental factors A_2 and B_2.

Table 4 shows the correlation factors A_2 and B_2 together with the coefficient of determination R^2 for the trend lines of all fuels. As R^2 is almost 1.000, it can be stated that the trend lines describing the experimental data curve fit well.

In the next stage, a correlation between the new factors A_2 and B_2 and the old factors A_1 and B_1 has to be established. The B_2 factor appears constant and distributed randomly around a fixed value, thus no fuel parameter dependency is assumed at this stage. However, for A_2 it can be seen that HVO has the lowest parameter of 51.3 followed by diesel of 53.1 and 53.5–53.8 for the three neat FAMEs, respectively. The A_2 value for the B50 series are always between B0 and the equivalent B100 fuel. The density dependency has been expressed in the following equation:

$$A_2 = A_1 \cdot X_2 \cdot \rho^z \tag{5}$$

where z is the weighting factor of the fuel density effecting the penetration and X_2 is a proportional factor to compensate the higher injection pressure and chamber density. Rearranging and linearising the equation and taking the 47.58 for A_1 and A_2 values from Table 4 the equation can be written as:

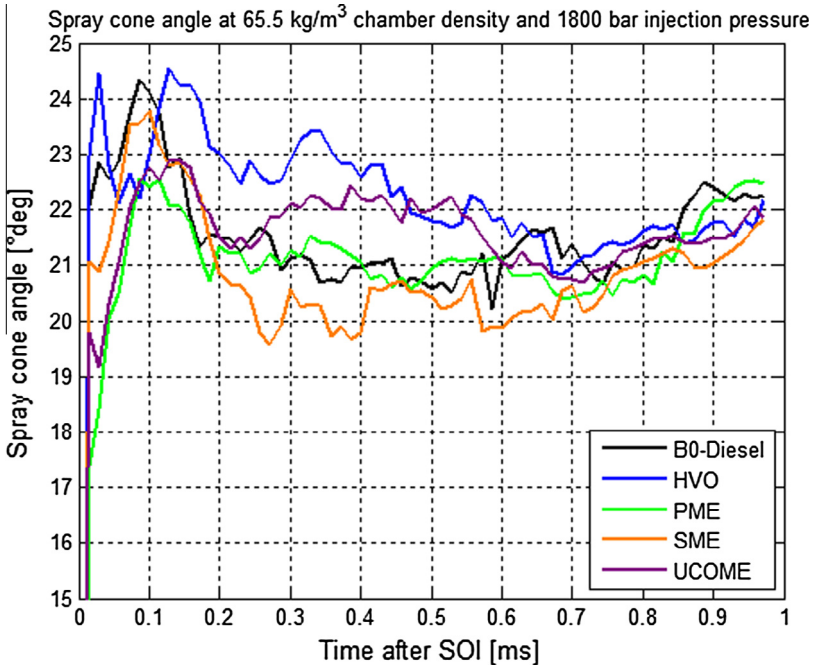

Fig. 13. Spray cone angle evolution of tested fuels at 100 °C chamber temperature.

Please cite this article in press as: Bohl T et al. Macroscopic spray characteristics of next-generation bio-derived diesel fuels in comparison to mineral diesel. Appl Energy (2016), http://dx.doi.org/10.1016/j.apenergy.2016.10.082

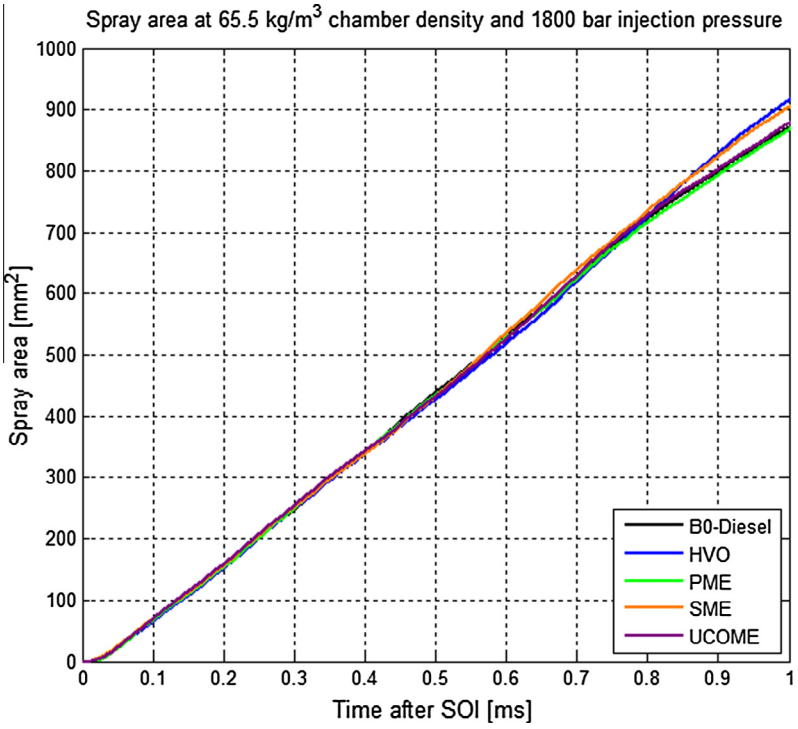

Fig. 14. Spray area of tested fuels at 100 °C chamber temperature.

$$ln\left(\frac{A_2}{A_1}\right) = ln(X_2) + z \cdot \ln(\rho) \quad (6)$$

$$y = b + m \cdot x$$

This equation with the ratio of A_2/A_1 has to be valid for all fuels in Table 5 and one constant for X_2 and z representing the whole range of fuels has to be determined.

Fig. 9 shows the graphical solution and a linear trend is evident.

The trend line has a coefficient of determination of 0.9481, which is considered high and can sufficiently indicate a linear correlation. The slope of the trend line is 0.3387 and the y-axis intersect is -2.1562. Thus z and X_2 can be determined as:

$$m = z = \underline{0.3387} \quad (7)$$

$$b = ln(X_2) \rightarrow X_2 = e^{-2.1562} = \underline{0.1158} \quad (8)$$

The new and modified penetration equation can now be written as:

$$S_2 = 2.95 \cdot \left(\frac{\Delta P}{\rho_g}\right)^{\frac{1}{4}} \cdot \sqrt{d_0} \cdot 0.1158 \cdot \rho^{0.3387} \cdot t^{0.5432} \quad (9)$$

$$for\ t \geqslant t_b$$

The exponential factor for the time has changed from 0.5 to 0.5432 and is the average value of B_2 in Table 6.

The new factors A_2 and B_2 are now valid for all fuels at higher injection pressures and chamber densities of around 1800 bar and 60–70 kg/m^3, respectively. The new spray models have been plotted in Figs. 10 and 11 for B0 diesel and the four neat biofuels (only every third data point has been plotted to have a better distinction between the curves). It can be concluded that the modified model matches the experimental data very well for different types of fuels with changing fuel densities.

For validation purposes the model has been applied to the spray tests at low injection pressure of 600 bar. As nozzle geometry, fuel density and chamber density are constant throughout the tests just ΔP changes from 1730 bar to 530 bar giving a new, smaller pre-exponential factor for A_2.The results of experimental and modelled penetration data have been shown for B0 and PME, representatively for all fuels (see Fig. 12).

Table 8
Injected mass and energy of different fuels at 1800 bar and 0.6 ms injection duration.

Fuel	Injected mass (mg)	Calorific value (kJ/kg)	Injected energy (J/stroke)
B0 Reference diesel	6.32	42,853	271
HVO B100	5.61	43,902	246
PME B100	7.00	37,320	261
SME B100	6.97	37,230	259
UCOME B100	6.92	37,200	257

3.2.3. Spray cone angle

Fig. 4 presents the spray cone angle for the five test fuels at 1800 bar injection pressure, 70 bar backpressure and 100 °C chamber temperature and 80 °C fuel temperature. All tested fuels show a very similar cone angle with HVO being slightly higher. UCOME, PME and SME fuel show a slow rise in cone angle just after the start of injection. A jet-shaped spray at the very beginning is assumed to be caused by the higher viscosity of the fuel.

Table 7 presents the average cone angle of all neat fuels for 600 bar and 1800 bar injection pressure. With higher injection pressures the cone angle increases slightly. The higher pressure causes higher kinetic energy in the spray and smaller fuel droplets are formed, which are more likely to atomise and scatter in the chamber. At 600 bar injection pressure, HVO provides the highest cone angle of all fuels followed by the three FAMEs and B0 with very similar cone angles of about 20 degree. The high cone angle of HVO can be explained with the low viscosity of the fuel.

At 1800 bar, the average cone angle for the three FAMEs is smaller than HVO and B0 which is in line with the observations of Valentino et al. and Guan et al. which reported that those fuels with higher fuel viscosities have reduced spray cone angles [22,29].

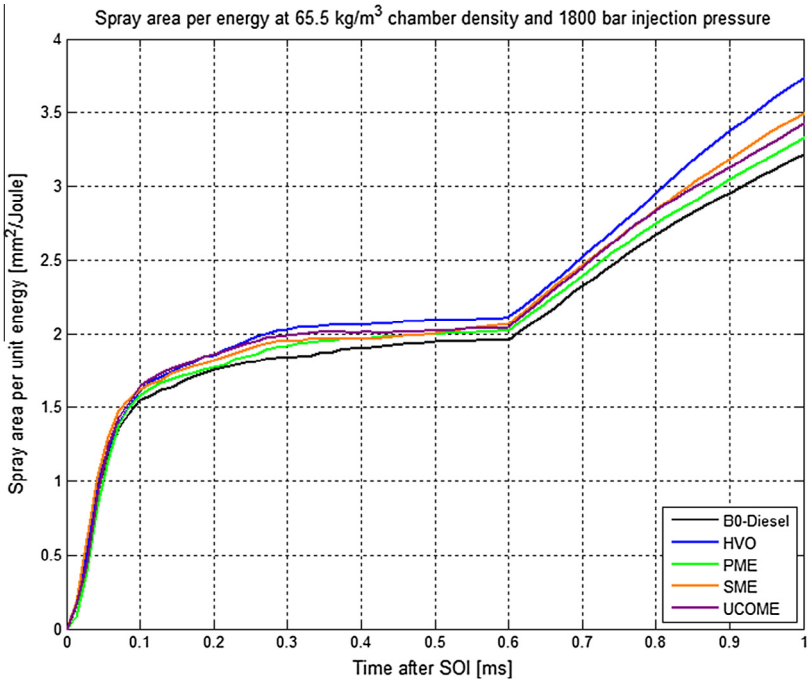

Fig. 15. Energy specific projected spray area for tested fuels at 1800 bar.

3.2.4. Projected spray area

Fig. 14 presents the projected spray area of all five test fuels at 1800 bar injection pressure and 100 °C chamber temperature. The spray area is an indicator of the characteristics of the fuel-air mixing process itself since a greater spray area would be expected to correspond to a more widely distributed plume of fuel droplets. A generally linear trend as a function of time can be observed for all fuels. From this it can be concluded that for the same injection conditions, all these fuels have similar air-fuel mixing properties. Nevertheless, whilst the injection events observed for the three FAMEs and B0 resulted a large area caused by a relatively longer spray tip penetration (see Fig. 14), the HVO fuel achieved the equivalent area as a result of a larger cone angle than the other fuels (see Fig. 13). This is a critical difference in a real-world engine context as the direct injection of HVO fuel would be expected to penetrate less and potentially result in less wall impingement. As a result, this would then be expected to have corresponding impacts on the observed exhaust gas emissions associated with spray-wall interaction such as CO, uHCs and PM.

Nevertheless, it must be noted that in an internal combustion engine, injection events are typically based on a volume of fuel injected and different fuels usually have their own corresponding densities and heating values. In this basis, the total amount of energy injected per event and the global air/fuel ratio is different for each fuel. Based on the calorific value, the total injected energy has been estimated for each fuel. The injected mass and corresponding energy of each test fuels are shown in Table 8.

To analyse the importance of this, Fig. 15 presents the spray area per Joule (energy specific spray area) as a function of time for injection events obtained at 1800 bar injection pressure, 70 bar backpressure and 100 °C chamber temperature. At the start of the injection, all fuels follow the same trend and with commencing fuel injection the specific projected spray area develops faster for HVO followed by the three FAMEs and is less distinctive for B0.

Whilst, the calorific value of HVO is very high, the main reason for HVO showing the largest energy specific spray area is its low liquid density resulting in less fuel and therefore less energy being injected over a set duration. The energy specific spray area of conventional diesel is least developed as the liquid density of the fuel is high resulting in a higher injection mass, furthermore the high heating value further increases the effect as less volume of fuel is required to achieve the same power output as would be required for the tested biodiesels.

The spray area can be considered as indicator for the quality of the fuel-air mixing process, it can be concluded that HVO shows a very high tendency to achieve a good initial fuel-air mixture distribution and thus resulting in a higher premix portion. It is this portion which is chiefly responsible for dictating when the fuel ignites, nevertheless HVO has a high cetane number which will promote ignition and potentially resulting in less time for a premixed phase to develop.

For SME, PME and UCOME the trend will be similar and the observed higher ratio of spray area per unit energy will yield a more premixed combustion event than mineral diesel. Nevertheless, the high liquid viscosity of these fuels typically results in larger fuel droplets thus diminishing the fuel-air mixture distribution area and therefore the potential for a longer premixed combustion phase.

4. Conclusion

In this work, the spray characteristics of next-generation biofuels have been investigated and differences between these fuels and conventional mineral diesel have been identified. The following conclusions can be drawn from this work:

1. High liquid density fuels such as FAMEs proved to have longer spray penetrations than mineral diesel, whereas HVO has a shorter penetration.
2. At modern engine relevant high injection pressures, the Hiroyasu and Arai penetration model proved sufficiently valid in its general assumptions however some of its key parameters required modification and different liquid fuel densities proved to have a significant effect on the penetration.

Please cite this article in press as: Bohl T et al. Macroscopic spray characteristics of next-generation bio-derived diesel fuels in comparison to mineral diesel. Appl Energy (2016), http://dx.doi.org/10.1016/j.apenergy.2016.10.082

3. A new spray model has been developed based on Hiroyasu & Arai valid for diesel-like alternative fuels, such as FAME and HVO, at chamber densities of about 60–70 kg/m^3 and injection pressures of 600–1800 bar including an exponential density contribution of 0.3094.
4. The spray cone angle of HVO proved larger at 600 and 1800 bar compared to the other fuels. The higher liquid viscosity FAMEs show very similar cone angles to mineral diesel, but the angle just after injection increased slowly resulting in a jet-shaped spray pattern until the spray breakup point.
5. The spray area proved identical for all fuels at the same injection conditions. However, with different liquid fuel densities and heating values the injection timing on an engine would need to be changed to achieve the same power output.
6. HVO appears to have the best preconditions for a high-quality air-fuel premixing process.

Acknowledgement

The authors kindly thank Cummins Ltd UK for their financial and technical contribution towards this work. Also, this study was supported by EPSRC scholarship and loan of the camera equipment (EP/J500288/1). Data supporting this publication is openly available under an 'Open Data Commons Open Database License'. Additional metadata are available at: http://dx.doi.org/10.17634/154300-32. Please contact Newcastle Research Data Service at rdm@ncl.ac.uk for access instructions.

References

[1] IEA. World Energy Outlook; 2009.
[2] IEA. World Energy Outlook 2012. 2012 [cited 2013 02.04.2013]; Available from: <http://www.iea.org/publications/freepublications/publication/German.pdf>.
[3] IEA. CO2 emissions from fuel combustion. 2010 [cited 2013 02.04.2013]; Available from: <http://www.iea.org/co2highlights/co2highlights.pdf>.
[4] Council Directive, DIRECTIVE 2003/30/EC OF THE EUROPEAN PARLIAMENT AND OF THE COUNCIL of 8 May 2003 on the promotion of the use of biofuels or other renewable fuels for transport, in L 123/42. 2003, European Parliament: Official Journal of the European Union.
[5] Ajanovic A, Haas R. Economic challenges for the future relevance of biofuels in transport in EU countries. Energy 2010;35(8):3340–8.
[6] Tan PQ et al. Exhaust emissions from a light-duty diesel engine with Jatropha biodiesel fuel. Energy 2012;39(1):356–62.
[7] Agarwal AK. Biofuels (alcohols and biodiesel) applications as fuels for internal combustion engines. Prog Energy Combust Sci 2007;33(3):233–71.
[8] Gill SS et al. Combustion characteristics and emissions of Fischer-Tropsch diesel fuels in IC engines. Prog Energy Combust Sci 2011;37(4):503–23.
[9] Balat M, Balat H. Progress in biodiesel processing. Appl Energy 2010;87(6):1815–35.
[10] Atadashi IM, Aroua MK, Aziz AA. High quality biodiesel and its diesel engine application: a review. Renew Sustain Energy Rev 2010;14(7):1999–2008.
[11] Lee CS, Park SW, Kwon SI. An experimental study on the atomization and combustion characteristics of biodiesel-blended fuels. Energy Fuels 2005;19(5):2201–8.
[12] Alptekin E, Canakci M. Characterization of the key fuel properties of methyl ester-diesel fuel blends. Fuel 2009;88(1):75–80.
[13] Li Y. et al. Comparative Experimental Study on Microscopic Spray Characteristics of RME, GTL and Diesel. SAE Technical Paper; 2010. 2010-01-2284.
[14] Subramanian KA, Lahane S. Comparative evaluations of injection and spray characteristics of a diesel engine using karanja biodiesel–diesel blends. Int J Energy Res 2013;37(6):582–97.
[15] Gao Y et al. Experimental study of the spray characteristics of biodiesel based on inedible oil. Biotechnol Adv 2009;27(5):616–24.
[16] Kuti OA et al. Characterization of spray and combustion processes of biodiesel fuel injected by diesel engine common rail system. Fuel 2013;104:838–46.
[17] Suh HK, Roh HG, Lee CS. Spray and combustion characteristics of biodiesel/diesel blended fuel in a direct injection common-rail diesel engine. J Eng Gas Turbines Power 2008;130(3):032807.
[18] Grimaldi C, Postrioti L, Experimental comparison between conventional and bio-derived fuels sprays from a common rail injection system. SAE Technical Paper; 2000. 2000-01-1252.
[19] Aatola H. et al. Hydrotreated vegetable oil (HVO) as a renewable diesel fuel: trade-off between NOx, particulate emission, and fuel consumption of a heavy duty engine. SAE Technical paper; 2008. 2008-01-2500.
[20] Park SH et al. A study on the fuel injection and atomization characteristics of soybean oil methyl ester (SME). Int J Heat Fluid Flow 2009;30(1):108–16.
[21] Mancaruso E, Sequino L, Vaglieco BM. First and second generation biodiesels spray characterization in a diesel engine. Fuel 2011;90(9):2870–83.
[22] Guan L et al. Effect of di-n-butyl ether blending with soybean-biodiesel on spray and atomization characteristics in a common-rail fuel injection system. Fuel 2015;140:116–25.
[23] Hiroyasu H, Kadota T, Arai M. Supplementary comments: fuel spray characterization in diesel engines. Combust Model Reciproc Eng 1980:369–408.
[24] Naber J, Siebers, DL. Effects of gas density and vaporization on penetration and dispersion of diesel sprays. SAE Technical Paper; 1996. 960034.
[25] Dent JC. A basis for the comparison of various experimental methods for studying spray penetration. SAE Technical Paper; 1971. 710571.
[26] Hay N, Jones PL. Comparison of the various correlations for spray penetration. SAE Technical Paper; 1972. 720776.
[27] Wakuri Y et al. Studies on the penetration of fuel spray in a diesel engine. Bull JSME 1960;3(9):123–30.
[28] Schihl P, Bryzik W, Atreya A. Analysis of current spray penetration models and proposal of a phenomenological cone penetration model. SAE Technical Paper; 1996. 960773.
[29] Valentino G et al. Biodiesel/mineral diesel fuel mixtures: spray evolution and engine performance and emissions characterization. Energy 2011;36(6):3924–32.